Spatially resolved Raman studies of diamond films grown by chemical vapor deposition

Joel W. Ager III, D. Kirk Veirs,* and Gerd M. Rosenblatt
Center for Advanced Materials, Materials Sciences Division, Lawrence Berkeley Laboratory, University of California, Berkeley, California 94720
(Received 22 October 1990)

The frequency and line shape of the diamond Raman line are examined in detail for a series of microwave-plasma-assisted chemical-vapor-deposition films grown on Si. The Raman lines in the films appear at higher frequency (shifts of up to 3 cm^{-1}) than that of natural diamond and the observed lines are symmetric with broader linewidths than that of natural diamond, ranging from 5.7 to 17.1 cm^{-1}. In addition, the line frequencies and linewidths are correlated; the films with the highest vibrational frequencies have the largest linewidths. The data include single-point measurements on eight films grown under different conditions as well as 500 data points from different positions on a single film that were obtained in a spatially resolved Raman experiment. Several mechanisms for the frequency shift and the correlation of the linewidth with frequency are considered including phonon confinement, residual stress, and defect scattering. Contrary to the observations, Raman line shapes computed from the phonon-confinement model (which has been used successfully to model Raman scattering in microcrystalline Si and GaAs), using phonon-dispersion curves for diamond from the literature, are highly asymmetric at the linewidths observed. It is concluded that the observed shifts in the diamond Raman line do not arise from phonon confinement alone and arise primarily from compressive stress. The line broadening also is not produced by phonon confinement alone and may arise from decreasing phonon lifetime associated with scattering from defects or from an inhomogeneous stress distribution in the films. The observed correlation between Raman line frequency and width suggests that the degree of compressive stress may be associated with the density of microcrystalline defects.

I. INTRODUCTION

Polycrystalline diamond thin films are now grown routinely from gaseous precursors by a variety of methods [chemical vapor deposition (CVD), hot filament, flame, etc.]. These films possess the physical properties of bulk diamond such as high thermal conductivity and hardness. Current and suggested applications of these films include heat sinks, tool coatings, x-ray and IR optics, abrasives, and fast semiconductor devices. Spear[1] and Yarbrough and Messier[2] have recently reviewed the preparation, analysis, and potential uses of diamond films.

Raman spectroscopy is important in the characterization of diamond thin films; observation of the sharp diamond Raman line at approximately 1333 cm^{-1} is definitive evidence of diamond growth. Many workers have reported Raman spectra from diamond films.[3] Recently, Knight and White[4] have measured Raman spectra from diamond films deposited by different methods on a wide variety of substrates. Bonnot[5] has used a Raman microprobe to measure polarized Raman spectra of individual crystallites in a diamond thin film as a function of crystallite orientation.

The Raman line of natural diamond occurs at 1332.5 cm^{-1} and has a width of 2 cm^{-1}.[6] In polycrystalline diamond films, the Raman linewidths are typically broader, ranging from 5–15 cm^{-1}. The observed Raman linewidth depends on the film preparation conditions and has been proposed to be related to the degree of structural order in the film microcrystallites.[4,5] In addition, the line is often shifted relative to that of natural diamond; this has been attributed to the presence of compressive or tensile stress in the film.[4] In lower-quality films, broad features centered at approximately 1580 and 1360 cm^{-1} also appear in the Raman spectrum; these are due to amorphous carbon.[7]

We present here Raman spectra from a series of CVD-grown diamond thin films and spatially resolved data from a single film. We observe a correlation between the linewidth and frequency of the diamond Raman line in the films studied. We examine explanations for this correlation based on strain, defect, and phonon-confinement models.

II. EXPERIMENT

A. Diamond-film preparation

All films studied were grown by microwave-plasma-assisted CVD on Si substrates scratched with diamond paste. The conditions for the films produced at Lawrence Berkeley Laboratory (LBL) are shown in Table I. The cross-sectional area of the plasma produced by the LBL apparatus was smaller than the substrate (10-mm-diam Si wafers). As a result, the films are spatially inhomogeneous, generally with more growth toward the edge of the wafer. In addition, many of the LBL films are not continuous. Typical scanning-electron-microscopy (SEM) images are shown in Fig. 1. Two continuous films with thicknesses of 4 and 20 μm from a commercial source[8] were also studied.

 ©1991 The American Physical Society

TABLE I. Growth conditions and Raman measurements of CVD diamond thin films. Growth conditions for the commercial films were not available.

Film	Substrate T (°C)	Pressure (Torr)	% CH_4	Time (h)	Raman frequency (cm^{-1})	Raman linewidth (cm^{-1})
1	975	140	1.2	1.5	1332.9	5.7
2	975	85	1.2	1.5	1333.4	6.7
3	975	95	0.8	1.5	1333.2	8.5
4	975	85	0.9	1.0	1334.7	10.5
5	975	85	0.7	1.0	1334.6	11.0
6	975	85	0.4	1.0	1335.3	12.3
7	975	85	0.4	1.0	1334.5	15.2
8	975	85	0.9	1.0	1335.4	17.1
225-5 commercial					1332.9	6.7
217-4 commercial					1332.5	5.9
Synthetic type-II*a* diamond					1332.4	2.4

B. Raman apparatus

Raman spectra are excited with the 488-nm line of an Ar^+ laser. Both the laser- and collected-light polarizations can be controlled for polarization studies. With the 85-mm focusing lens used here, the spot size of the laser on the films is 6 μm. The laser is incident at 70° from the normal and the scattered light is collected normal to the sample by a 50-mm $f/1.3$ camera lens.

The scattered light is imaged through an interference filter and polarization analyzer onto the entrance slit of a 0.64-m single monochromator. The dispersed light is detected by a microchannel plate photomultiplier with a position-sensitive resistive anode (1024×1024 pixel format; each physical pixel is 25 μm×25 μm). With the 2400-groove/mm grating used here, one pixel on the detector corresponds to 0.4 cm^{-1}. The slit width is typically 120 μm, which corresponds to an instrument-

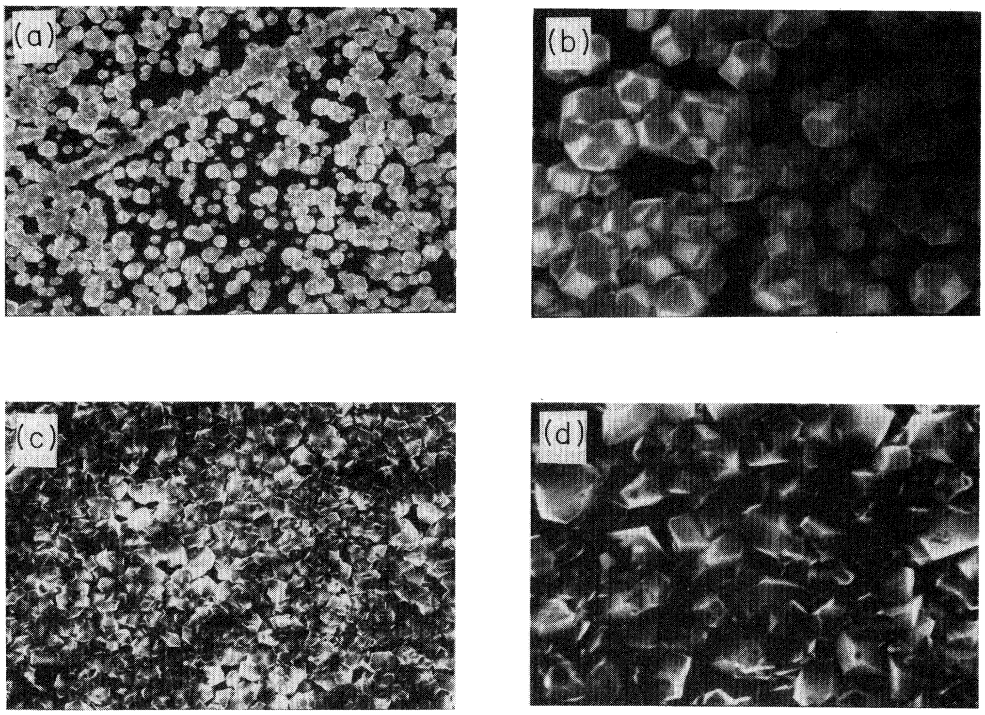

FIG. 1. SEM photos of sample 1: (a) and (b) 2500× and 7500× images of mostly isolated, cubo-octahedral crystallites typical of the center of the sample; (c) and (d) more irregular, partially fused crystallites from the edge of the sample at the same magnifications as (a) and (b), respectively. The diagonal line of fused crystallites in (a) is caused by the presence of a scratch in the Si substrate. The Raman linewidth measured in the center of sample 1 is narrower than that measured near the edge (cf. Fig. 5).

limited linewidth of 2 cm^{-1}. The observed Raman linewidths from the films are at least three times this value and are not significantly instrument broadened.

Typical collection times are 100 s at a laser power of 10 mW. Line frequencies and widths are calculated by fitting to a Lorentzian line shape with a linear background term. There is excellent agreement between the observed and calculated line shapes and the statistical uncertainties of the fit are much smaller than the estimated systematic errors. Line frequencies are calibrated by comparison with a Ne spectrum;[9] our estimate of the accuracy of the line-center measurements is ± 0.3 cm^{-1}.

We have described previously the use of a two-dimensional detector to obtain multiple, spatially resolved Raman spectra simultaneously along an illuminated line on the sample;[10] only a brief description of the method will be given here. The laser is focused on the sample by a cylindrical lens to form an illuminated line, which is imaged by the collection optics onto the entrance slit of the monochromator. Each of the 1024 rows of the detector contains the Raman spectrum from a corresponding point on the sample. Subsequent collection of a Ne calibration spectrum and data analysis[11] yield the frequencies of the Raman lines from the sample with an accuracy of 0.5 cm^{-1} (about one pixel). In the spatially resolved measurements reported here, the magnification of the collection optics was 8×, such that each row on the detector corresponded to the Raman spectrum from a 4-μm-long (33-μm effective pixel size divided by 8) by 15-μm-wide (120-μm slit width divided by 8) area of the sample.

III. RESULTS

A. Single-point measurements

Raman spectra showing the range of line shapes observed in this work are shown in Fig. 2. The Raman spectrum of a synthetic type-II*a* diamond is included for comparison. The linewidths in the diamond-film spectra are larger than that in the natural-diamond spectrum, and the peaks are shifted to higher frequency. The observed lines are fit well by symmetric, Lorentzian line shapes as shown in Figs. 2(b) and 2(c). There is no evidence of amorphous carbon, which exhibits broad bands around 1350 and 1560 cm^{-1}, in the Raman spectra of these as illustrated in Fig. 3. The measured Raman frequencies and linewidths from ten films are tabulated in Table I. The Raman lines in the films are at higher frequencies (up to 1335 cm^{-1}) than that of natural diamond and the observed linewidths are larger, ranging from 5.7 to 17.1 cm^{-1}. The observed linewidths are graphed versus the peak frequency in Fig. 4. The frequencies and linewidths are correlated, with the films having the largest shifts to higher Raman frequencies having the largest linewidths.

B. Spatially resolved Raman measurements

The microwave plasma used to make the LBL films was small compared to the diameter of the substrate (10 mm), and many of the films have inhomogeneous cover-

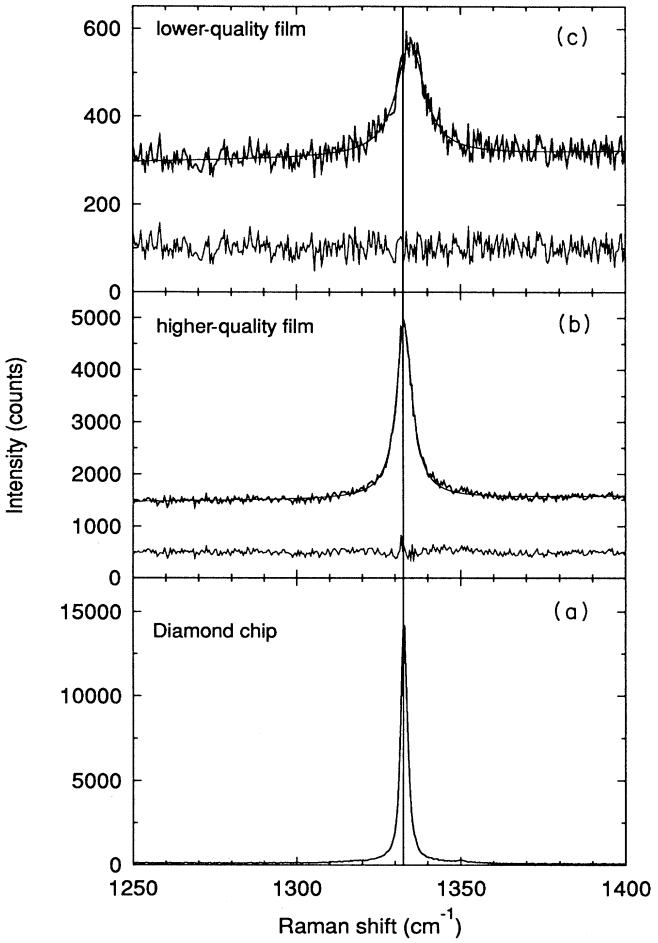

FIG. 2. Raman spectra of diamond: (a) synthetic, type-II*a* diamond chip, single crystal; (b) center of sample 1, high-quality CVD film; (c) center of sample 4, lower-quality CVD film. The residuals from Lorentzian fits to the diamond Raman line are also shown in (b) and (c), offset by 500 and 100 counts, respectively.

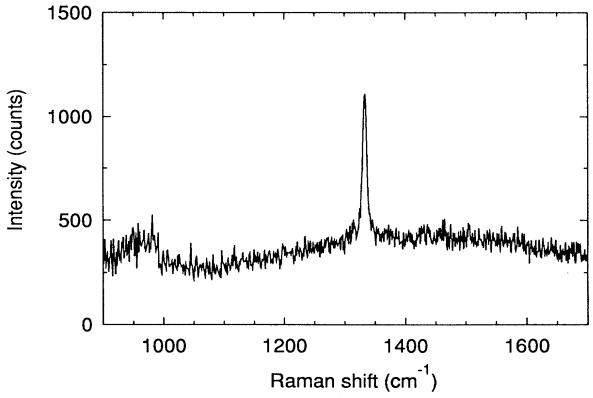

FIG. 3. Raman spectrum of sample 1. The broad feature at approximately 960 cm^{-1} is the second-order peak of the Si substrate. No amorphous-carbon features (broad bands at approximately 1560 and 1350 cm^{-1}) are observed.

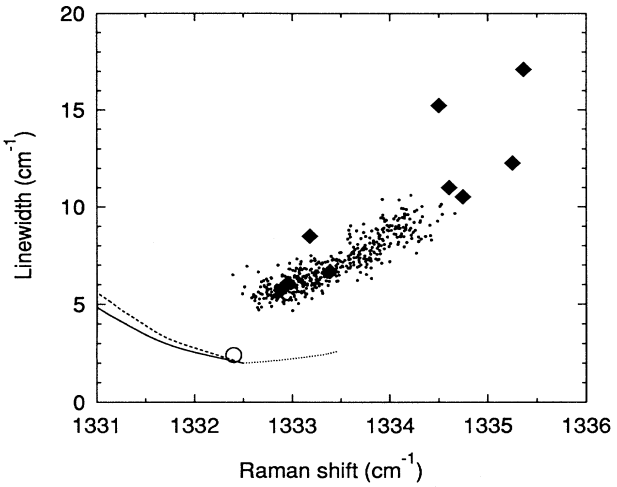

FIG. 4. Raman linewidth vs Raman line frequency for diamond: (circle) single-crystal diamond; (diamonds) single-point measurements from ten CVD diamond films; (dots) 500 spatially resolved measurements from sample 1; (solid line) phonon-confinement theory, case (a), averaged dispersion curve; (dotted line) theory, case (b), Δ_2' dispersion curve; (long dashes) theory, case (c), average of line shapes calculated with each of the seven diamond dispersion curves.

ages of diamond. Sample 1 is a good example; it has isolated diamond microcrystallites in the center of the film [Figs. 1(a) and 1(b)] and a higher density of partially fused crystallites near the side of the film [Figs. 1(c) and 1(d)]. A spatially resolved Raman image of sample 1 was obtained in an experiment using 400-mW laser power, a 1.5-h integration time, and 8× magnification. The central 500 rows of the data matrix were analyzed; these correspond to spatially resolved Raman spectra from 500 points along a 2-mm-long line on the sample. The sample was positioned such that the imaged area extended from areas of sparser to areas of denser diamond coverage. As described in detail previously,[10] Ne calibration data were collected to provide frequency calibration, independent of monochromator aberrations. The data were analyzed with CHEMMAP;[11] the results are shown in Fig. 5. The diamond linewidth is narrowest near the center of the sample (sparser coverage) and increases monotonically towards the edge of the sample (denser coverage). The Raman frequency is correlated with the linewidth; the line frequency is 1332.7 cm^{-1} in the center of the sample and increases to 1334.4 cm^{-1} at the edge of the imaged area. The linewidths and frequencies from the 500 spectra collected in the spatially resolved experiment are also included in Fig. 4; the correlation of linewidth and frequency found at different locations on this one film follows the same trend as the single-point measurements on different films.

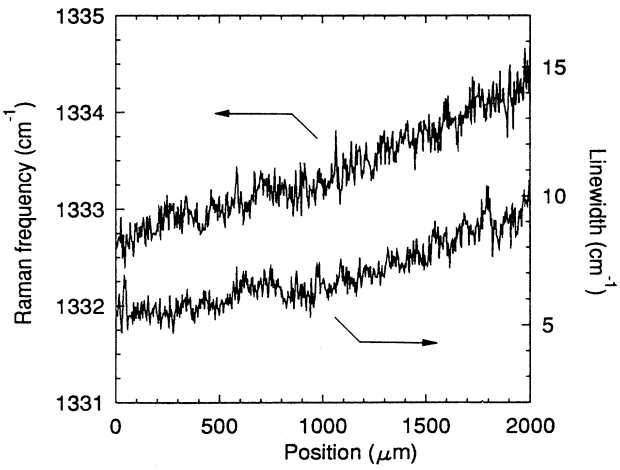

FIG. 5. Spatially resolved Raman results from sample 1. The observed Raman linewidth is smaller and the line frequency is closer to that of single-crystal diamond in the center of the sample (position, 0 μm). The Raman line broadens and shifts to higher frequency towards the edge of the sample. Figure 1 shows SEM photos of the center and edge regions of sample 1.

IV. DISCUSSION

A. Comparison to other studies

Large shifts of the Raman line in diamond films relative to that of natural diamond have been reported previously. Knight and White[4] report diamond Raman frequencies ranging from 1328 cm^{-1} (tungsten carbide substrate) to 1345 cm^{-1} (alumina substrate) and attribute the shifts to internal stresses in the films. However, they did not observe shifts in the Raman frequency for films grown on Si substrates. Bonnot[5] reports a diamond Raman frequency range of 1323–1336 cm^{-1} and a linewidth range of 9–22 cm^{-1} from a series of CVD films on Mo and Si substrates. Some of the films in that study have substantial amounts of amorphous carbon, as indicated by the appearance of broad bands at 1360 and 1550 cm^{-1} in the Raman spectrum. Asymmetric line shapes are also reported. In addition, in microprobe experiments with single microcrystallites, the peak frequencies of crystals with the (100) face parallel to the substrate were shifted to lower frequency, while peaks from crystals with two (100) and two (111) faces parallel to the substrate were shifted to higher frequency. Bonnot suggests that larger compressive stresses occur when the crystal grows in the latter orientation. The shifts to lower frequencies are attributed qualitatively to phonon confinement (this model is considered below), in analogy to similar behavior in microcrystalline semiconductors.

Although many authors have reported shifts and broadening of the diamond line in diamond films, we know of no reports of a correlation between linewidth and frequency.

B. Stress

Several groups have measured the shift in the Raman frequency of single-crystal diamond as a function of pressure (hydrostatic stress) in diamond-anvil cells.[12–14] In these experiments, the triple degeneracy of the zone-center phonon is retained. There is good agreement on

the magnitude of the shift as a function of pressure, 2.9 cm^{-1}/GPa. Grimsditch *et al.*[15] measured the effect of uniaxial stress on the zone-center phonon of single-crystal diamond. Uniaxial stress causes a combination of hydrostatic and pure shear strains; the latter split the triply degenerate zone-center phonon into a singlet (vibration parallel to stress axis) and a doublet (vibration perpendicular to stress axis). The relative magnitude of the shift for the two components is dependent on the direction of the stress. The Raman spectra of the two components can be distinguished by polarization analysis. The linewidth of the two components does not change with increasing uniaxial stress; this is also true for the single line observed in hydrostatic-stress experiments.[12]

C. Phonon-confinement model

Richter *et al.*[16] have developed a model (known as the spatial-correlation or phonon-confinement model) to explain the observed shift to lower frequency and broadening of the Raman line in microcrystalline Si. The model has been used to fit Raman line shapes and estimate microcrystallite sizes in Si (Refs. 17–19) and GaAs.[20–22] Very recently, LeGrice *et al.*[23] have used a combination of stress and phonon-confinement models to estimate internal stresses and domain sizes from Raman line frequencies and linewidths observed in diamond films. The phonon-confinement model is based upon the fact that, in an infinite crystal, crystal momentum conservation limits Raman spectroscopy to observing phonons at the center of the Brillouin zone ($\mathbf{q}\approx\mathbf{0}$). However, in an imperfect crystal, phonons can be confined in space by microcrystallite boundaries or defects. This results in uncertainty in the phonon momentum, allowing phonons with $\mathbf{q}>\mathbf{0}$ to contribute to the Raman signal. In the limit of small microcrystallites or very high defect densities, phonons from the entire Brillouin zone contribute to the Raman signal. The model is outlined briefly below.

The wave function of a phonon with wave vector $\mathbf{q}_0$ in an infinite crystalline lattice is

$$\Phi(\mathbf{q}_0,\mathbf{r})=u(\mathbf{q}_0,\mathbf{r})e^{i\mathbf{q}_0\cdot\mathbf{r}}, \tag{1}$$

where $u(\mathbf{q}_0,\mathbf{r})$ has the periodicity of the lattice. If the phonon is confined to a sphere of diameter L (Campbell and Fauchet[18] have discussed the effects of different confining shapes such as cylinders, etc.), the phonon wave function becomes

$$\Psi(\mathbf{q}_0,\mathbf{r})=W(\mathbf{r},L)\Phi(\mathbf{q}_0,\mathbf{r})=\Psi'(\mathbf{q}_0,\mathbf{r})u(\mathbf{q}_0,\mathbf{r}), \tag{2}$$

where $W(\mathbf{r},L)$ describes the confinement and $\Psi'(\mathbf{q}_0,\mathbf{r})=W(\mathbf{r},L)e^{i\mathbf{q}_0\cdot\mathbf{r}}$. The confined-phonon wave function $\Psi'(\mathbf{q}_0,\mathbf{r})$ is expressed as a Fourier series,

$$\Psi'(\mathbf{q}_0,\mathbf{r})=\int d^3q\, C(\mathbf{q}_0,\mathbf{q})e^{i\mathbf{q}_0\cdot\mathbf{r}}, \tag{3}$$

where the Fourier coefficients $C(\mathbf{q}_0,\mathbf{q})$ are given by

$$\begin{aligned}C(\mathbf{q}_0,\mathbf{q})&=\frac{1}{(2\pi)^3}\int d^3r\,\Psi'(\mathbf{q}_0,\mathbf{r})e^{-i\mathbf{q}_0\cdot\mathbf{r}}\\&=\frac{1}{(2\pi)^3}\int d^3r\,W(\mathbf{r},L)e^{-i(\mathbf{q}-\mathbf{q}_0)\cdot\mathbf{r}}\end{aligned} \tag{4}$$

and are essentially the Fourier transform of the confining function. The wave function of the confined phonon is a superposition of plane waves with wave vectors $\mathbf{q}$, centered around $\mathbf{q}_0$. The Raman line shape is constructed by superimposing Lorentzian line shapes (with the linewidth of the infinite crystalline material) centered at $\omega(\mathbf{q})$, weighted by the wave-vector uncertainty caused by the confinement:

$$I(\omega)\cong\int\frac{d^3q\,|C(0,\mathbf{q})|^2}{[\omega-\omega(\mathbf{q})]^2+(\Gamma_0/2)^2}, \tag{5}$$

where $\omega(\mathbf{q})$ is the phonon-dispersion curve, Γ_0 is the natural linewidth, and $\mathbf{q}_0=\mathbf{0}$ for zone-center Raman scattering and the integration is over the entire Brillouin zone. As $L\to\infty$, $C(0,\mathbf{q})=\delta(\mathbf{q})$ and $I(\omega)$ is a Lorentzian centered at $\omega(0)$ (the Raman frequency) with a linewidth of Γ_0. Various choices can be made for the confining function $W(\mathbf{r},L)$, as discussed by Campbell and Fauchet.[18] In this work we use a Gaussian confinement:

$$\begin{aligned}W(\mathbf{r},L)&=\exp\left[\frac{-8\pi^2r^2}{L^2}\right],\\|C(0,\mathbf{q})|^2&\cong\exp\left[\frac{-q^2L^2}{4}\right],\end{aligned} \tag{6}$$

with $\mathbf{q}$ in units of $2\pi/a$ where a is the lattice constant (3.56 Å for diamond) and L and r are in units of a (3.56 Å for diamond).

In Si and GaAs, all branches of the phonon-dispersion curves decrease similarly in the vicinity of the Γ point. Therefore the three-dimensional (3D) Brillouin-zone integration in Eq. (5) can be approximated with a one-dimensional integration in a spherical Brillouin zone, using an appropriately averaged dispersion curve:

$$I(\omega)\cong\int_0^1\frac{dq\,\exp(-q^2L^2/4)4\pi q^2}{[\omega-\omega(q)]^2+(\Gamma_0/2)^2}, \tag{7}$$

where $\omega(q)$ is an approximate one-dimensional phonon-dispersion curve. When the momentum uncertainty is convoluted with the dispersion curves (which contain the $\mathbf{q}$ dependence of the phonon frequency), the predicted Raman line shape asymmetrically broadens and the maximum shifts to lower frequency as L decreases.[16–22]

Diamond has the same symmetry as Si and the lattice dynamics of the two crystals are similar in the $\Gamma\xrightarrow{K}X$ and $\Gamma\xrightarrow{\Lambda}L$ directions;[24] in these branches the phonon frequency decreases as $\mathbf{q}$ increases. However, in the $\Gamma\xrightarrow{\Delta}X$ or [001] direction in diamond, the highest-frequency dispersion curve, $\Delta_2'(O)$, has a shallow maximum near the Γ point[25] as shown in Fig. 6; the effect of this curve on the predictions of the phonon-confinement model is discussed below.

Figure 7 schematically shows the effect of wave-vector uncertainty by graphing $W(r,L)$ and $|C(0,q)|^2$ for $L=100$, 50, and 20 Å and Gaussian confinement. We present three sets of line-shape calculations in which different assumed one-dimensional phonon-dispersion curves are used. For case (a) we use a dispersion curve

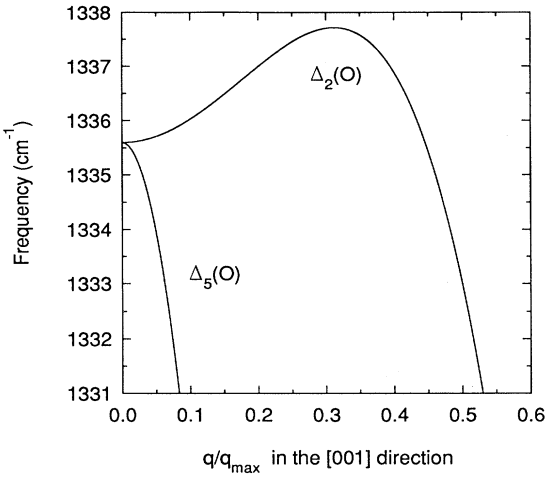

FIG. 6. Detail of (001) phonon-dispersion curves for diamond from Ref. 25. The $\Delta_5(O)$ curve decreases away from the Γ point; this is similar to the behavior of all the dispersion curves in Si. The $\Delta_2'(O)$ curve in diamond has a shallow maximum. When used in the phonon-confinement theory, the two curves predict qualitatively different line shapes as a function of L, the confining length (cf. Fig. 8).

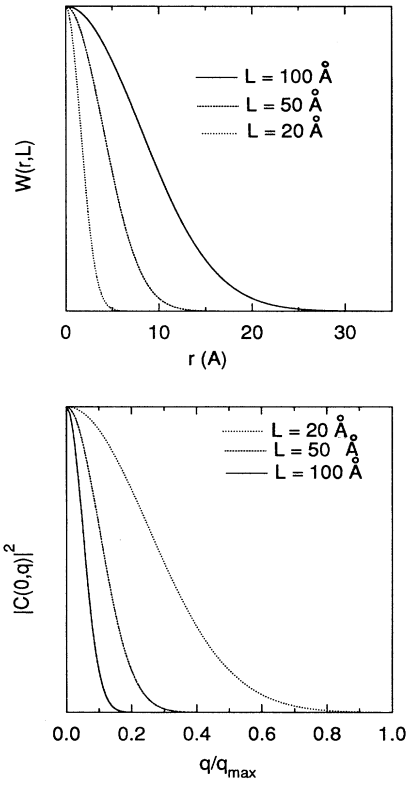

FIG. 7. $W(\mathbf{r},L)$ and $|C(0,\mathbf{q})|^2$ for Gaussian confinement from Eq. (6): (solid line) $L=100$ Å; (dashed line) $L=50$ Å; (dotted line) $L=20$ Å. Confining the phonon to a smaller volume in real space leads to a larger uncertainty in its momentum. For $L=20$ Å, phonons from the entire Brillouin zone contribute to the Raman signal.

that is an empirical average of the optical-branch dispersion curves from Tubino and Birman[25] for which the phonon frequency decreases away from the Γ point [$\Lambda_1(O)$, $\Lambda_3(O)$, $\Delta_5(O)$, $\Sigma_1(O)$, $\Sigma_2(O)$, and $\Sigma_3(O)$, using the notation of Warren *et al.*[24]]. We assume the form[20] $\omega(q)=A+B\cos(q\pi)$ where $A=1241.25$ cm^{-1} and $B=91.25$ cm^{-1}; the shape of this averaged curve is similar to that used in Si and GaAs phonon-confinement calculations. For case (b), we assess the effect of the $\Delta_2'(O)$ high-frequency dispersion curve that has the shallow maximum by evaluating Eq. (7) with it alone. In case (c) we attempt to approximation a true 3D Brillouin-zone integration by calculating separate phonon-confinement line shapes for each dispersion curve (seven in all) from Refs. 24 and 25 using Eq. (7) and then summing them with the appropriate degeneracy weighting [$\Lambda_3(O)$ and $\Lambda_5(O)$ are doubly degenerate[24]] to produce an average line shape.

The calculated line shapes for cases (a) and (b) are shown in Fig. 8 and the results for all three cases are summarized in Table II for a range of L from 20 to 200 Å. Cases (a) and (c) gave similar results (cf. Table II and Fig. 4), suggesting that using an averaged one-dimensional dispersion curve is a good approximation for phonon-confinement calculations in systems where most of the dispersion curves behave similarly in the vicinity of the Γ point. In cases (a) and (c), the line broadens asymmetrically and the maximum shifts to lower frequency; the behavior is similar to that calculated for Si and GaAs.[16–22] Case (b) produces qualitatively different behavior; the maximum shifts slightly to higher frequency with decreasing L and the broadening is more symmetric and smaller in magnitude for the same L as compared to case (a).

D. Comparison to experiment

The linewidths (full width at half maximum) and frequencies predicted by the phonon-confinement model for the three cases are shown in Fig. 4 along with the observed values. When the averaged dispersion curve [case (a)] is used, linewidths on the order of 5 cm^{-1} (the minimum observed in the films) are predicted for $L\approx 100$ Å. The predicted shift of the peak maximum to lower frequency is not observed in the films studied here. When the $\Delta_2'(O)$ dispersion curve [case (b)] is used, the calculations predict that the linewidth will increase as the frequency increases, in qualitative agreement with the experimental data. However, the observed linewidths are systematically larger and the shifts to higher frequency are much larger than predicted by the calculation.

The phonon-confinement model, especially in cases (a) and (c), predicts strongly asymmetric line shapes at values of L less than about 100 Å. Although some slightly asymmetric lines are observed here (and have been reported for diamond films by others[5]), the observed asymmetries are much smaller than those predicted by the model for a given linewidth. For example, the observed spectrum from sample 1 in Fig. 2(b) and the calculated spectrum in Fig. 8(a) for $L=100$ Å both have a linewidth of 5.7 cm^{-1}. However, while the observed spectrum is

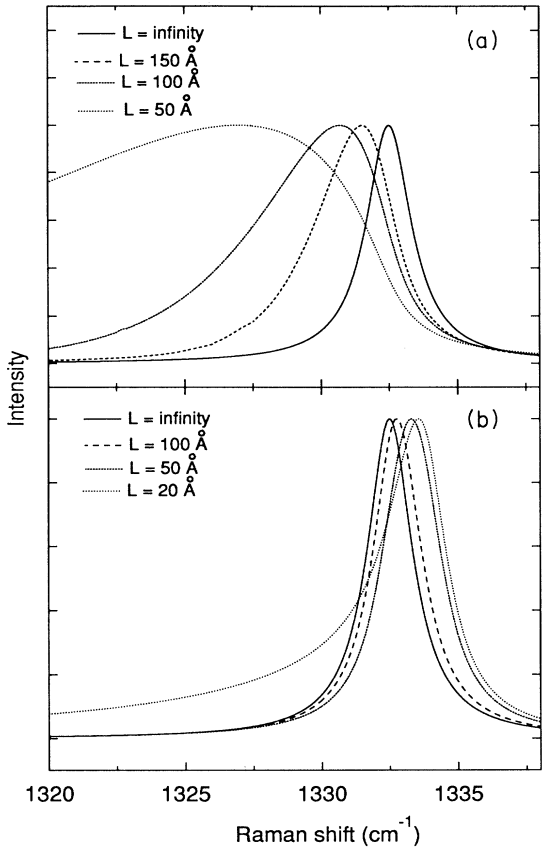

FIG. 8. Calculated Raman line shapes from the phonon-confinement theory for different values of L, the confinement length: (a) results of case (a) calculations using an averaged one-dimensional dispersion curve; (solid line) $L=\infty$, no confinement; (long dashes) $L=150$ Å; (short dashes) $L=100$ Å; (dots) $L=50$ Å; (b) results of case (b) calculations using the $\Delta_2'(O)$ dispersion curve (cf. Fig. 6); (solid line) $L=\infty$, no confinement; (long dashes) $L=100$ Å; (short dashes) $L=50$ Å; (dots) $L=20$ Å. The case (c) calculation (see text) produced line shapes similar to those of case (a). The values of L used in (a) and (b) are different.

symmetric, as can be seen by the flat residual trace from the Lorentzian fit, the predicted line shape is clearly asymmetric. The disagreement between the observed and calculated line shapes for a given linewidth becomes more marked at larger linewidths (smaller values of L). This is in contrast to the results on the microcrystalline Si and GaAs (Refs. 16–22) where there is good agreement between the predicted phonon-confinement and observed Raman line shapes. Because the diamond line shapes we observe are much more symmetric than predicted by the model, we conclude that the linewidth broadening for the films in this study does not arise from phonon confinement alone.

The lack of agreement between the observed line shapes and those predicted by the phonon-confinement model leads to consideration of alternative mechanisms for the Raman frequency shift and the broadening. The most likely cause of the shift of the diamond Raman line to higher frequency appears to be strain caused by compressive stress. The largest shift to higher frequency observed in this work, 2.5 cm^{-1}, would correspond to a stress of 0.9 GPa. This would appear to be a reasonable value for residual stress in a diamond film and is very small compared to the tensile and shear strengths of diamond, which are 190 and 121 GPa, respectively. Stress in the films might be caused by the difference in thermal expansion of diamond and Si. As the film and substrate cool from the growth temperature of 900 °C, the Si substrate, which has a large thermal expansion coefficient, contracts somewhat more than the diamond film, perhaps producing compressive stress in the film.

We can suggest two potential mechanisms for the broadening of the Raman line in the films compared to that of natural diamond. The first is lifetime broadening. The Raman linewidth of natural diamond is related to the lifetime of the phonon created in the Raman process. The primary broadening mechanism in a perfect crystal is decay of the optical phonon into two acoustic phonons with opposite wave vectors.[26] However, in imperfect crystals such as those in polycrystalline diamond films, the phonon created in the Raman process can also decay at grain boundaries and at defect sites, further reducing the lifetime and broadening the Raman line. If phonon

TABLE II. Results of phonon-confinement calculations. Case (a) uses an averaged phonon-dispersion curve, case (b) uses the $\Delta_2'(O)$ curve only, and case (c) uses all the curves separately and then averages the calculated lines (see text).

	Case (a)		Case (b)		Case (c)	
L (Å)	Frequency (cm^{-1})	Linewidth (cm^{-1})	Frequency (cm^{-1})	Linewidth (cm^{-1})	Frequency (cm^{-1})	Linewidth (cm^{-1})
∞	1332.5	2.0	1332.5	2.0	1332.5	2.0
200	1331.88	2.71			1331.88	2.97
150	1331.50	3.45			1331.60	3.60
120	1331.13	4.44			1331.25	4.70
100	1330.75	5.59	1332.80	2.12	1330.94	5.78
70	1329.38	9.82	1333.12	2.30	1329.69	10.2
50	1327.05	17.7	1333.32	2.44	1328.10	17.8
40			1333.39	2.51		
30			1333.46	2.60		
20			1333.60	3.00		

lifetimes determine the linewidth, one would then expect the Raman line in microcrystalline diamond films to broaden with increasing defect density and with decreasing crystallite size. The line shape would be Lorentzian with a larger linewidth, as was observed in the spectra of the diamond films. Such broadening has been observed in microcrystalline Si.[16] In the diamond films, the typical dimensions of the microcrystallites are large (approximately 1 μm, cf. Fig. 1) compared to the phonon coherence length (approximately 200 Å) associated with lifetime-broadened linewidth of a few cm^{-1}. One concludes that, if the linewidth is due to lifetime broadening, the shortened lifetime must arise from scattering from defect sites as opposed to grain boundaries.

A second possible mechanism is that the observed broadening arises from averaging over many different microcrystallites. The Raman spectra of these translucent films are produced by scattering from many microcrystallites, each of which might have a different amount of internal stress and hence a different Raman frequency. A vertical stress gradient in the microcrystallites might be produced by differences in lattice size and thermal expansion between diamond and Si. In addition, the microcrystallites can relax by breaking or buckling from the substrate. Effects such as these lead to vertical stress gradients during epitaxial growth of GaAs.[27] A stress distribution of 2–6 GPa across the microcrystallites sampled in the laser beam would be consistent with the observed linewidths. However, in order to produce the observed Lorentzian line shape (cf. Fig. 2), the distribution of microcrystallites having different internal stresses must also be close to Lorentzian.

We can suggest two possible explanations for the observed correlation of Raman linewidth and frequency shift in the films studied. One possibility is that the width of the stress distribution in the large number of microcrystallites sampled by the laser increases with the maximum stress on any microcrystallite. That is, the films with Raman lines close to that of natural diamond might be relatively homogeneous and have a narrow internal-stress distribution and linewidth, while films with large shifts of the Raman line to higher frequency might be more heterogeneous and have a much wider stress distribution and linewidth. Another possibility is that factors that produce high compressive internal stress (which is proportional to the peak shift) also produce a high defect density (which proportionally increases the linewidth). In this case, films with small amounts of internal stress would have a low concentration of defects and correspondingly narrow linewidths, while films with large amounts of internal stress would have a higher defect density and larger linewidths.

V. SUMMARY AND CONCLUSIONS

Spatially resolved Raman results from a diamond thin film are presented, along with single-point measurements from eight other films grown under a variety of microwave-plasma-assisted CVD conditions. In the films studied, the diamond Raman line is shifted to higher frequency with respect to natural diamond and a correlation is found between the linewidth and frequency. The broadened lines remain symmetric and Lorentzian. Several explanations for these observations are considered. The most probable is that the frequency shift is due to compressive stress and that the linewidth increase arises from scattering of the optical phonon by defects and/or from an inhomogeneous stress distribution among the microcrystallites in the sampled volume. The observed correlation between Raman linewidth and frequency might arise from a correlation between defect density and internal compressive stress or from a correlation between the magnitude of the stress and the range of stresses experienced by microcrystallites in the sampled volume of the film. The phonon-confinement model, which successfully explains Raman line shapes in microcrystalline Si and GaAs,[16–22] predicts broadened, asymmetric lines shifted to lower frequency (up to 5 cm^{-1}) or slightly shifted to higher frequency (up to 1 cm^{-1}). The observed line shapes, frequencies, and linewidths in the diamond films examined here (up to 1 cm^{-1}) cannot be explained with the phonon-confinement model alone.

ACKNOWLEDGMENTS

We thank Marilee Brewer and Ian Brown (LBL), for providing the films used in this study and Kannan Krishnan (LBL), Peter Yu (LBL and University of California at Berkeley), and Lawrence Pan (Stanford Synchrotron Research Laboratory) for helpful discussions. This work was supported by the Director, Office of Energy Research, U.S. Department of Energy, under Contract No. DE-AC03-76SF00098.

*Present address: Los Alamos National Laboratory, Los Alamos, NM 87545.

[1]K. E. Spear, J. Am. Ceram. Soc. **72**, 171 (1989).
[2]W. A. Yarbrough and R. Messier, Science **247**, 688 (1990).
[3]W. A. Yarbrough and R. Messier, Science **247**, 688 (1990), and references therein.
[4]D. S. Knight and W. B. White, J. Mater. Res. **4**, 385 (1989).
[5]A. M. Bonnot, Phys. Rev. B **41**, 6040 (1990).
[6]S. A. Solin and A. K. Ramdas, Phys. Rev. B **1**, 1687 (1970).
[7]R. J. Nemanich, J. T. Glass, G. Lucovsky, and R. E. Shroder, J. Vac. Sci. Technol. A **6**, 1783 (1988).
[8]Crystallume, 3180 Porter Rd., Suite 2, Palo Alto, CA 94301.
[9]*American Institue of Physics Handbook,* edited by D. E. Gray (McGraw-Hill, New York, 1963) pp. 7-48–7-55.
[10]D. K. Veirs, J. W. Ager III, E. T. Loucks, and G. M. Rosenblatt, Appl. Opt. **29**, 4969 (1990).
[11]E. T. Loucks and D.K. Veirs, computer code CHEMMAP (University of California, Berkeley, CA, 1990).
[12]S. S. Mitra, O. Brafman, W. B. Daniels, and R. K. Crawford, Phys. Rev. **186**, 942 (1969).
[13]H. Boppart, J. van Staaten, and I. F. Silvera, Phys. Rev. B **32**, 1423 (1985).

[14]M. Hanfland, K. Syassen, S. Fahy, S. G. Louie, and M. L. Cohen, Physica B+C **139/140B**, 516 (1986).
[15]M. H. Grimsditch, E. Anastassakis, and M. Cardona, Phys. Rev. B **18**, 901 (1978).
[16]H. Richter, Z. P. Wang, and L. Ley, Solid State Commun. **39**, 625 (1981).
[17]J. Gonzalez-Hernandez, G. H. Azarbayejani, R. Tsu, and F. H. Pollack, Appl. Phys. Lett. **47**, 1350 (1985).
[18]I. H. Campbell and P. M. Fauchet, Solid State Commun. **58**, 739 (1986).
[19]P. M. Fauchet and I. H. Campbell, Crit. Rev. Solid State Mater. Sci. **14**, S79 (1988).
[20]K. K. Tiong, P. M. Amirtharaj, F. H. Pollack, and D. E. Aspnes, Appl. Phys. Lett. **44**, 122 (1984).
[21]G. Braunstein, D. Tuschel, S. Chen, and S. T. Lee, J. Appl. Phys. **66**, 3515 (1989).
[22]M. Holtz, R. Zallen, O. Brafman, and S. Matteson, Phys. Rev. B **37**, 4609 (1988).
[23]Y. M. LeGrice, R. J. Nemanich, J. T. Glass, Y. H. Lee, R. A. Rudder, and R. J. Markunas, in *Diamond, Silicon Carbide, and Related Wide Bandgap Semiconductors,* edited by J. T. Glass, R. Messier, and N. Fujimori, MRS Symposia Proceedings No. 162 (Materials Research Society, Pittsburgh, in press).
[24]J. L. Warren, J. L. Yarnell, G. Dolling, and R. A. Cowley, Phys. Rev. **158**, 805 (1967).
[25]R. Tubino and J. L. Birman, Phys. Rev. B **15**, 5843 (1977). The increase in frequency near the Γ point is necessary to explain a sharp feature in the two-phonon spectrum at 2667 cm^{-1}.
[26]J. Menendez and M. Cardona, Phys. Rev. B **29**, 2051 (1984), and references therein.
[27]Y. Huang, P. Yu, M.-N. Charasse, Y. Lo, and S. Wang, Appl. Phys. Lett. **51**, 192 (1987); Y. H. Lo, M.-N. Charasse, H. Lee, D. Vakhshoori, Y. Huang, P. Yu, Z. Liliental-Weber, M. Werner, and S. Wang, in *Heteroepitaxy on Silicon II,* edited by C. C. Fan, J. M. Phillip, and B. Y. Tsaur (Materials Research Society, Pittsburgh, 1987).

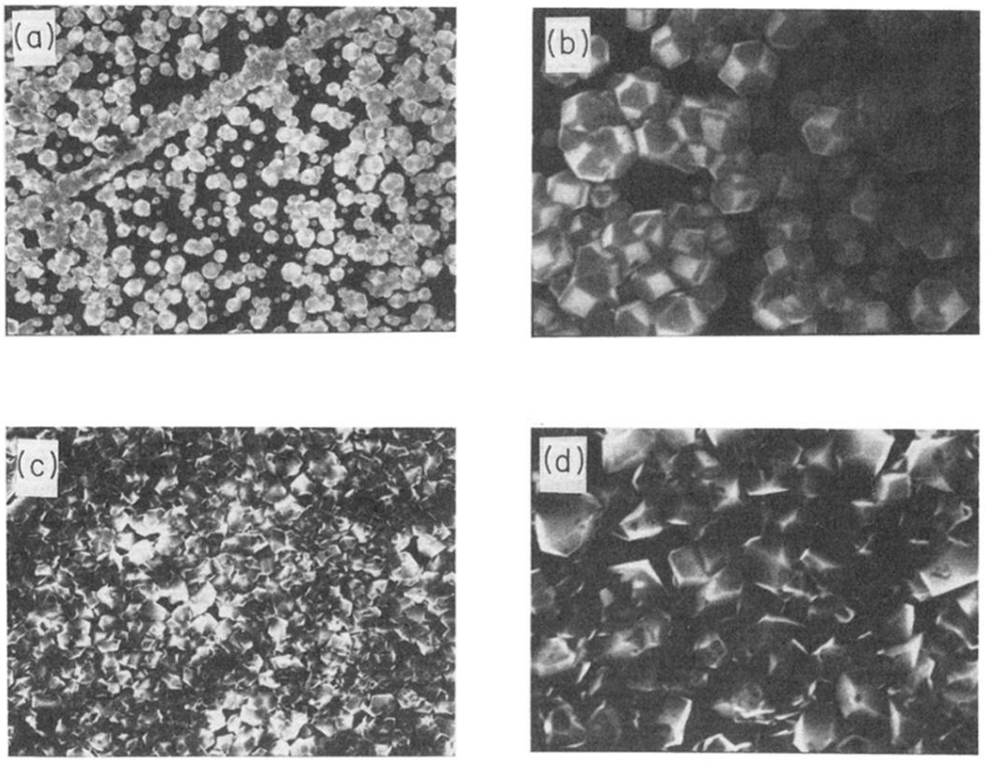

FIG. 1. SEM photos of sample 1: (a) and (b) 2500× and 7500× images of mostly isolated, cubo-octahedral crystallites typical of the center of the sample; (c) and (d) more irregular, partially fused crystallites from the edge of the sample at the same magnifications as (a) and (b), respectively. The diagonal line of fused crystallites in (a) is caused by the presence of a scratch in the Si substrate. The Raman linewidth measured in the center of sample 1 is narrower than that measured near the edge (cf. Fig. 5).